Proc. NIPR Symp. Polar Meteorol. Glaciol., 3, 58–78, 1990

EFFECTS OF RADIATION SCHEME ON THE SURFACE TEMPERATURE AND WIND OVER THE ANTARCTIC AND ON CIRCUMPOLAR LOWS

Kiyotaka SHIBATA and Masaru CHIBA

Meteorological Research Institute, 1–1, Nagamine, Tsukuba 305

Abstract: We have examined effects of radiation schemes including cloud emissivity on the surface temperature and wind over the Antarctic in May by performing one month integration of a global spectral model of the Meteorological Research Institute. It is found that radiation schemes have large effects on the surface and surface air temperatures; increase in longwave downward flux due to the improvement of radiation scheme directly results in temperature rises of surface and surface air. Above all, clouds play a crucial role in determining the surface temperature. When clouds are treated as non-black bodies, the surface temperature lowers through decrease in longwave downward flux. The surface temperature is found to be highly correlated to the surface pressure. When the surface temperature over the Antarctic rises, the surface pressure also rises, and the circumpolar lows move northward while weakening.

It is also shown that in the Antarctic the surface air is subject to large cooling owing to radiation and heat exchange with the cold surface; however, the cooling is compensated for by heating by adiabatic compression in down draft process and entrainment of upper warmer air. Surface wind speed is to a great degree affected by surface temperature, while surface wind direction is nearly independent of surface temperature.

1. Introduction

The Antarctic occupies a large area in the Southern Hemisphere, and hence general circulation models (GCMs) are suited for investigating the overall weather and climate of the Antarctic. However, it is not so easy to adequately simulate with GCMs the climate of the Antarctic in winter compared with that in summer. HERMAN and JOHNSON (1980), using a GLAS GCM, showed that the computed areally-averaged radiation balance at the surface is very close to the observed balance over the Antarctic Continent, but that the simulated surface temperature is too high, particularly in the Central Cold Core, which approximately corresponds to the region higher than 3000 m (DALRYMPLE, 1966). Similar overestimations of the surface temperature over the Antarctic can be seen in other GCMs (*e.g.*, MANABE and HAHN, 1981; PITCHER *et al.*, 1983; SCHLESINGER, 1984). It is worthwhile to point out that in most GCMs the circumpolar lows are also commonly weak in winter.

In winter it is found from observations that the surface heat balance over the Antarctic is maintained mainly by sensible heat and longwave radiation. In the Cold Central Core the sensible heat flux is comparatively small because of the weak surface wind; the monthly mean longwave net flux is about 15 W/m^2 (RUSIN,

1964; KUHN *et al.*, 1977). The longwave net flux is also still small in other regions except the coastal area, even though it shows gradual increases as the topographic height lowers. Therefore, to realistically simulate the climate of the Antarctic in winter the errors in computed longwave downward flux should be very small compared with the observed longwave downward flux.

The longwave radiation scheme of KATAYAMA (1972) (hereinafter referred to as KTY), which was used in an early version of the Meteorological Research Institute (MRI) global spectral model, is found to have large downward flux errors in the lower troposphere for the clear model atmospheres (SHIBATA *et al.*, 1988). On the other hand, SHIBATA and AOKI (1989) have developed a fairly accurate longwave radiation scheme by use of the multi-parameter random model (hereinafter referred to as MPR). When we incorporated this scheme in a global spectral model and ran the model for one month from May 1st 1984 to investigate impacts of the new radiation scheme, there were salient changes in the model climatology. For example, improvements can be seen in the northward shift of the baroclinic zone and separation of the tropospheric jet and stratospheric jet in the Southern Hemisphere. One of the factors responsible for these improvements can be ascribed to large increase (about 20 mb) in surface pressure on the Antarctic. We present here results and analyses of numerical experiments on one month integration, focusing on changes in the Antarctic and the region around it. The initial date of integration is May 1st 1984. Three runs are performed to examine not only effects of radiation schemes themselves, but also effects of cloud emissivity in longwave radiative transfer.

2. Brief Descriptions of Model and Experiments

The global spectral model used in this study is described in detail in CHIBA *et al.* (1986) and hence only a brief description is given here. The primitive equations are expressed as a series of spherical harmonics with the rhomboidal truncation of zonal wave number 24 (R24). Figure 1 shows the topography of the Antarctic, in which fine structures of the actual topography are smoothed because of the R24 wave truncation, and the steep inclinations in the coastal area are filtered out accordingly.

The model employs sigma, $\sigma = P/P_s$ (P_s: surface pressure), as the vertical coordinate; each sigma level is associated with a layer whose thickness is determined by the adjacent half sigma levels. The model has 11 sigma levels; the lowest level is 0.99, about 70 m height over the highland in the Antarctic. We tabulate the values of the sigma and half sigma levels in Fig. 2, in which dashed and solid lines represent the sigma and half sigma levels, respectively.

The major difference between the present model and that of CHIBA *et al.* (1986) is in the radiation scheme. The earlier model uses the longwave radiation scheme of KTY, whereas the present model employs the scheme of MPR. The comparison of two schemes is given in the next section. As for solar radiation the shortwave scheme is also improved to make it possible to treat multiple scattering in partially cloudy skies. When the cloud cover is 1.0, the present shortwave scheme is equivalent to that of LACIS and HANSEN (1974). However, this improvement only slightly affects the surface heat budget in the polar night season.

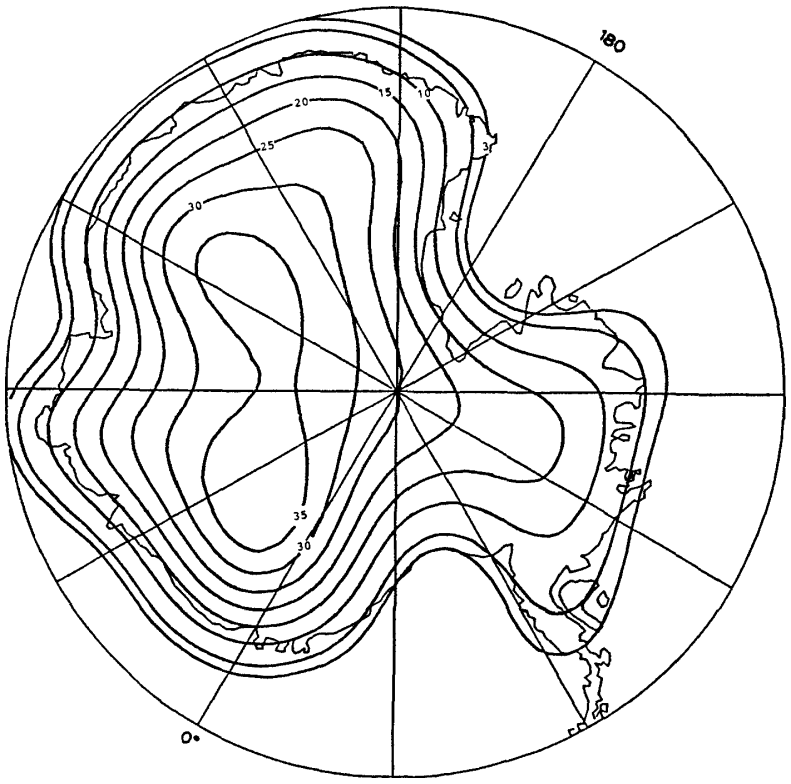

Fig. 1. Topography of the Antarctic represented in the spectral model of R24. Contours are drawn every 500 m, but the lowest contour is at 300 m height.

We carried out three runs A, B and C, which differ only in radiation processes. Runs A and C use the longwave scheme of MPR, while run B uses that of KTY as in the earlier version of CHIBA *et al.* (1986). In addition, we make further changes in run C: clouds are treated as non-black bodies; the shortwave scheme is modified as mentioned above; and albedos of snow and sea ice are changed. Table 1 shows differences in the radiation processes in the three runs.

The initial values are taken from the global analysis data on May 1st 1984 prepared by the Japan Meteorological Agency, and time integration is performed for

Table 1. Comparison of physical processes among the three runs, A, B, and C. LH denotes the shortwave radiation scheme of LACIS and HANSEN (1974).

	A	B	C	
Longwave radiation	MPR	KTY	MPR	
Shortwave	LH	LH	Modified LH	
Cloud emissivity	1.0	1.0	1.0	$T > -40°C$
			0.9	$-40°C > T > -50°C$
			0.7	$-50°C > T > -60°C$
			0.5	$-60°C > T$
Albedo				
sea ice	0.5	0.5	0.7	
land ice	0.7	0.7	0.7	
snow	0.7	0.7	0.83	

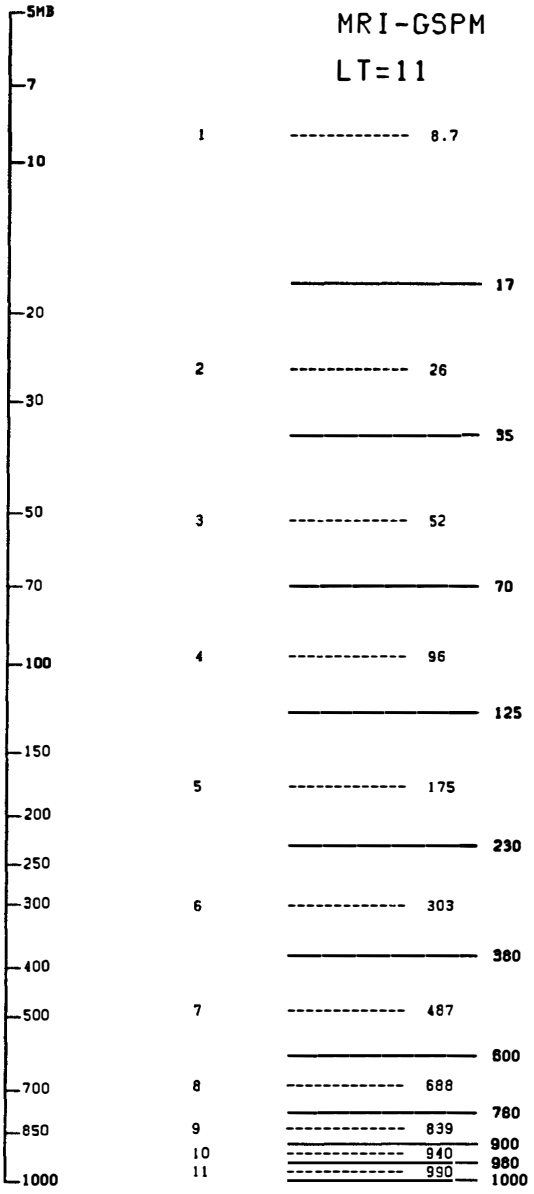

Fig. 2. Schematic figure of sigma and half sigma levels used in the spectral model of 11 layers. Unit of the sigma levels is 10^{-3}.

one month. The sea ice margin is set at 60°S.

3. Longwave Radiation Processes

3.1. Comparison of schemes

We use in the experiments two longwave radiation schemes. One is the KTY scheme; this is a numerical evaluation of the radiation chart of YAMAMOTO (1952). The other is the MPR scheme, in which the transmission function is represented with the multi-parameter random model based upon line-by-line calculations. There are too many differences between the two schemes to be explained here. We only show comparisons of errors in radiative fluxes and cooling rates for the clear model atmo-

Table 2. Comparison of longwave downward fluxes at various heights for the clear subarctic winter model atmosphere. LBL denotes line-by-line calculations, and MPR and KTY represent the scheme of SHIBATA and AOKI and that of KATAYAMA, respectively. The numbers in the second row for each altitude represent the difference from line-by-line calculations. (Fluxes of MPR and LBL, and those of KTY, are quoted from SHIBATA and AOKI (1989), and SHIBATA et al. (1988), respectively.)

Altitude (km)	Downward fluxes (W/m^2)		
	LBL	MPR	KTY
3.0	128.44	128.39	122.24
		−0.05	−6.20
2.2	142.54	142.24	136.30
		−0.30	−6.24
1.5	154.98	154.61	148.70
		−0.38	−6.28
0.7	164.34	164.08	156.89
		−0.26	−7.45
0.0	168.53	168.40	159.28
		−0.13	−9.25

spheres compiled by MCCLATCHEY *et al.* (1972).

From comparisons with the line-by-line calculations it is found that errors of the KTY scheme in flux are quite large, particularly in the downward flux in the lower troposphere of the subarctic winter and tropical model atmospheres (SHIBATA *et al.*, 1988), while errors of the MPR scheme are very small (SHIBATA and AOKI, 1989). For example, errors of the KTY and MPR schemes for subarctic winter are about 6–9 W/m^2 and less than 0.3 W/m^2, respectively, as shown in Table 2. The increase, 6–9 W/m^2, in downward flux due to improvement of the radiation scheme is greater than the radiative forcing due to CO_2 doubling (see *e.g.* CHOU and PENG, 1983; KIEHL and RAMANATHAN, 1983). As for cooling rates the KTY scheme yields large systematic underestimates in the upper troposphere for all the model atmospheres, while the MPR scheme yields relatively small errors there. In colder atmospheres than the subarctic winter model the difference between the two schemes is expected to be much larger because the transmittance function of the KTY scheme contains no temperature effect.

3.2. Cloud emissivity

In most GCMs high clouds are treated as non-black bodies. This is because observations and theoretical calculations (*e.g.*, YAMAMOTO *et al.*, 1970; LIOU, 1974; STEPHENS, 1978; GRIFFITH *et al.*, 1980) demonstrate that the cloud emissivity is less than unity for sufficiently small cloud liquid water (or ice) content (LWC). Thus, very small LWC clouds such as cirrus are substantially non-black. However, the treatment of high cloud emissivities varies from GCM to GCM; For example, emissivity is set to be a constant value of 0.5 (HOLLOWAY and MANABE, 1971) or a function of LWC (RAMANATHAN *et al.*, 1983). The former case is simple but may yield a large impact because the cloud emissivity varies stepwise from 1.0 for middle or low clouds to 0.5 for high clouds. The latter case is more realistic but the non-prognostic vari-

able LWC must be estimated. Since LWC decreases rapidly with height or temperature, we prescribed the cloud emissivity as a function of temperature; emissivity varies with temperature from 1.0 to 0.5, not abruptly, but rather gradually as depicted in Table 1.

In the radiative transfer scheme used in GCMs a cloud emissivity ε of one layer cloud is replaced with an effective amount of blackbody cloud A_e, which is related to the actual cloud amount A_c by $A_e=\varepsilon A_c$ (see *e.g.* HARSHVARDHAN *et al.*, 1987; RAMANATHAN *et al.*, 1983). The same relation holds for randomly overlapping clouds. Therefore, the difference in the effective cloud amount between run C and run A or B is due mainly to the difference in cloud emissivity.

4. Results of Run A

4.1. Surface sensible heat flux

Figure 3 shows the sensible heat flux in the third 10-day period over the Antarctic. Negative values in sensible heat flux mean that sensible heat flows from the atmosphere to the surface. In Fig. 3 sensible heat flux is very small, less than 20 W/m^2, in two regions; one is a region higher than about 3000 m in the East Antarctic, and the other is the region between 2000 m and 1500 m in the West Antarctic. We henceforth call the two regions, the "east plateau" and "west plateau", respectively. Around the two "plateaus" there are large sensible heat flux regions, beyond which sensible heat flux becomes positive value and sensible heat flows from the surface to the atmosphere. Longwave net flux is, similarly to the observations, nearly balanced with sensible heat flux over the Antarctic Continent (not shown).

4.2. Surface wind

The flow pattern of surface winds is depicted in Fig. 4. Surface wind directions roughly coincide with the climatological streamlines of MATHER and MILLER (1967) except in the coastal area. Both stream function and velocity potential of the surface wind approximately follow the topography, and their magnitudes are nearly similar to each other (not shown). Hence, the divergent wind and the rotational wind, which blow down and along the topographic contour, respectively, also have similar speeds. Surface air mass thus descends the topography while rounding it as seen in Fig. 4.

Figure 5 shows the isotachs of surface winds. The surface winds are always very weak on the "east plateau", and they decrease with topographic height; there blows almost no wind around the highest regions as seen in Fig. 4. On the "west plateau" the surface winds are also weak. The surface winds become strong away from the two "plateaus" and take maximum values on the sea ice slightly off the coast. According to observations (WELLER, 1969; SCHWERDTFEGER, 1970) katabatic winds take maximum values on the coast, and weaken rapidly in the sea ice region with distance from the coast. This weakening of katabatic winds is due to the occurrences of hydraulic jump or katabatic jump (BALL, 1956). In this model, however, the strong katabatic wind regions move toward the sea ice region. This is due partly to the very gradual inclinations of topography in the model; the topography does not show realistic steep inclinations in the coastal area, but quite gradual increases from coast to inland

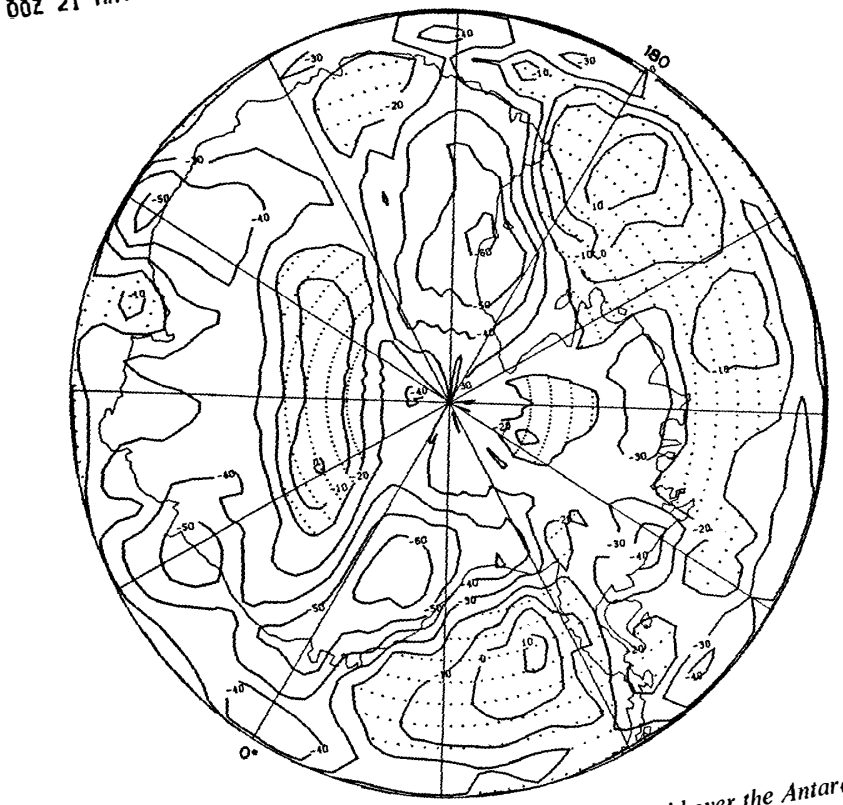

Fig. 3. Sensible heat flux in the third 10-day peroid over the Antarctic. Contour interval is 10 W/m², and the regions in which sensible heat fluxes are greater than −20 W/m² are dotted.

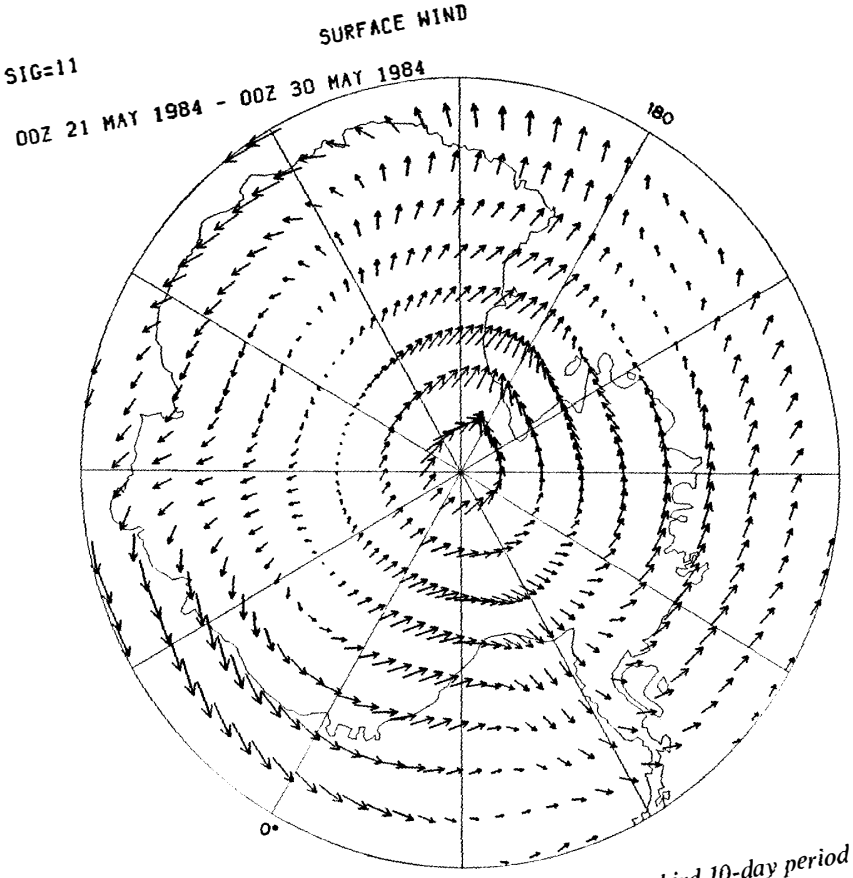

Fig. 4. Vector map of the surface wind in the third 10-day period over the Antarctic.

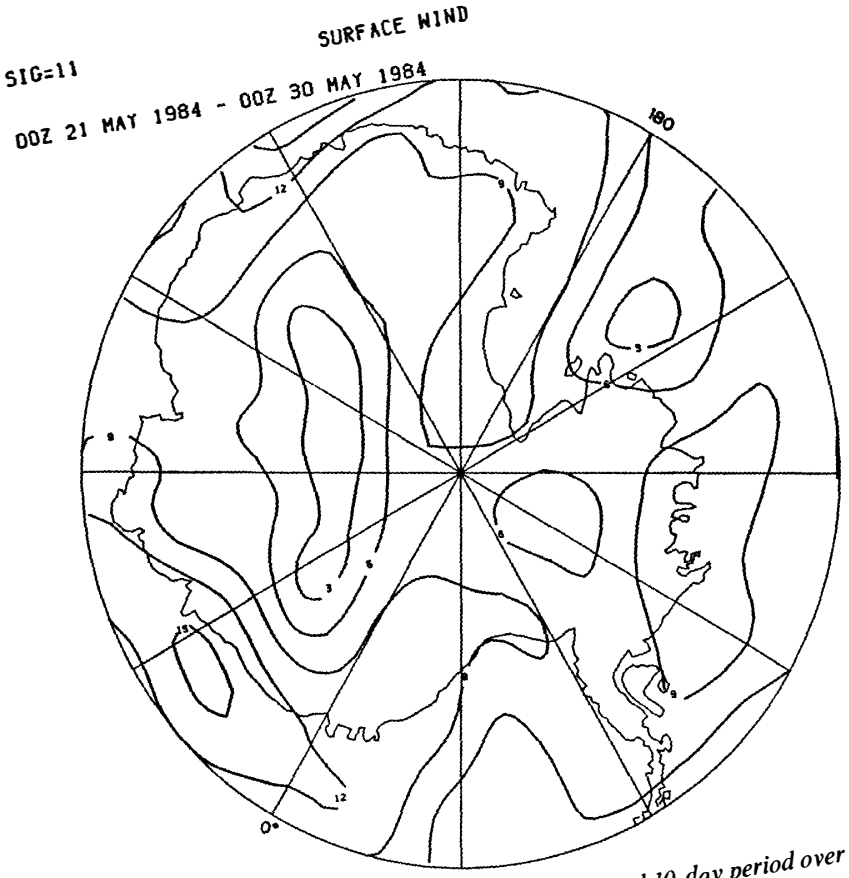

Fig. 5. Isotachs of the surface wind in the third 10-day period over the Antarctic. Contour interval is 3 m/s.

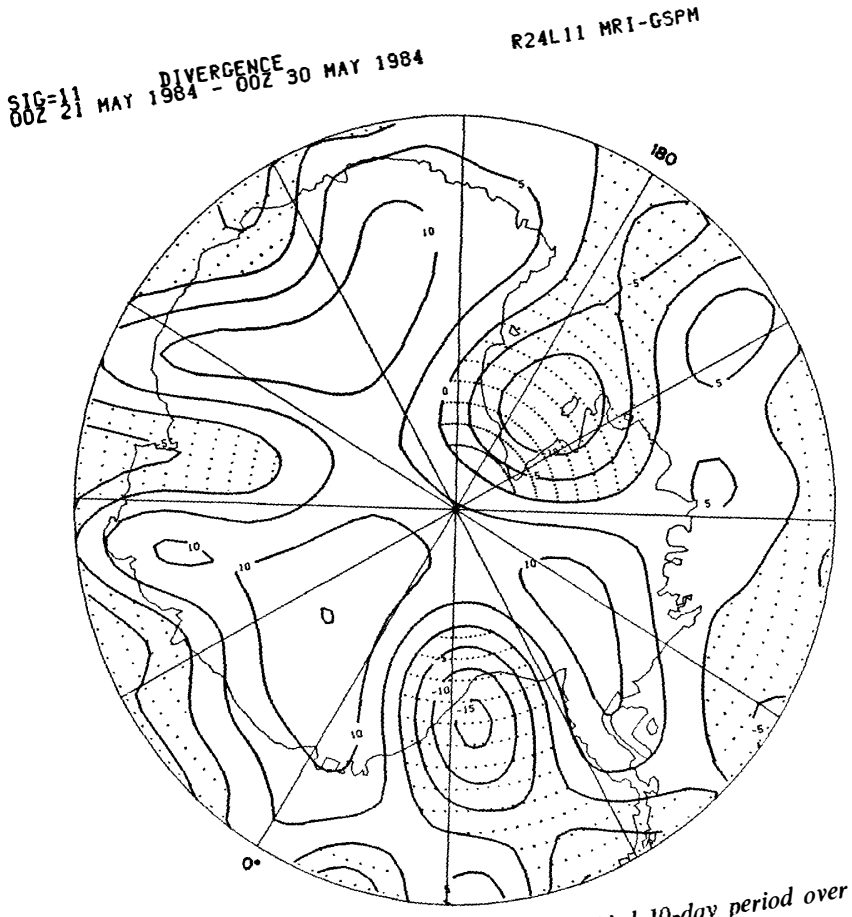

Fig. 6. Surface wind divergence in the third 10-day period over the Antarctic. Contour interval is 5×10^{-6} s^{-1}.

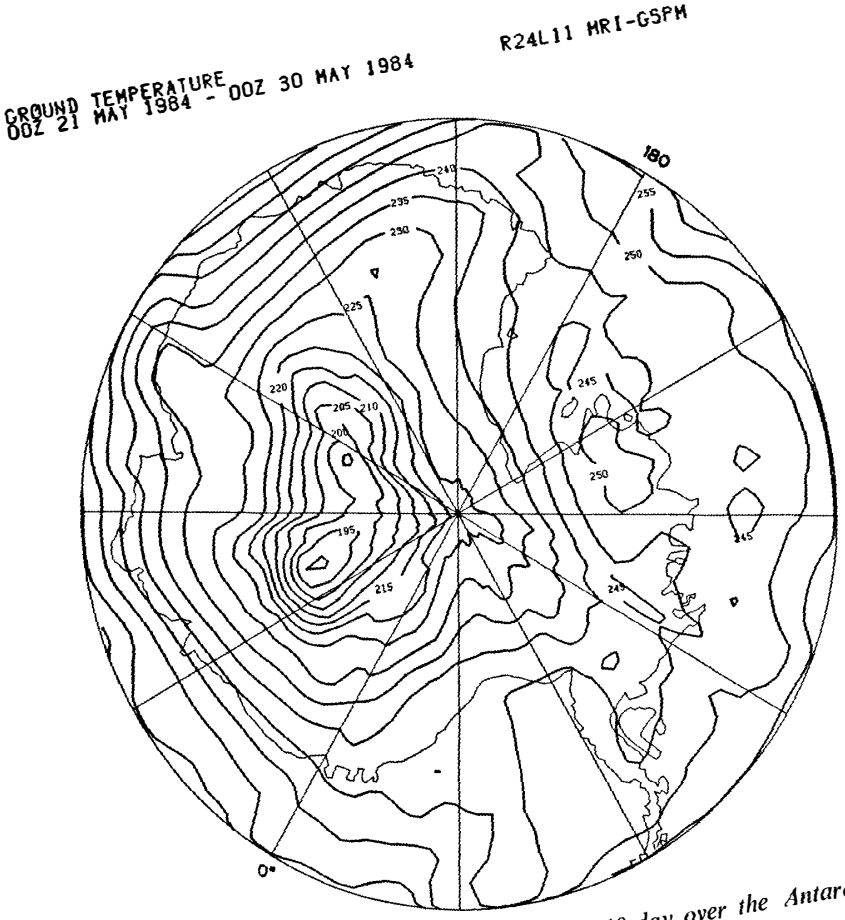

Fig. 7. Surface temperature in the third 10-day over the Antarctic. Contour interval is 5 K.

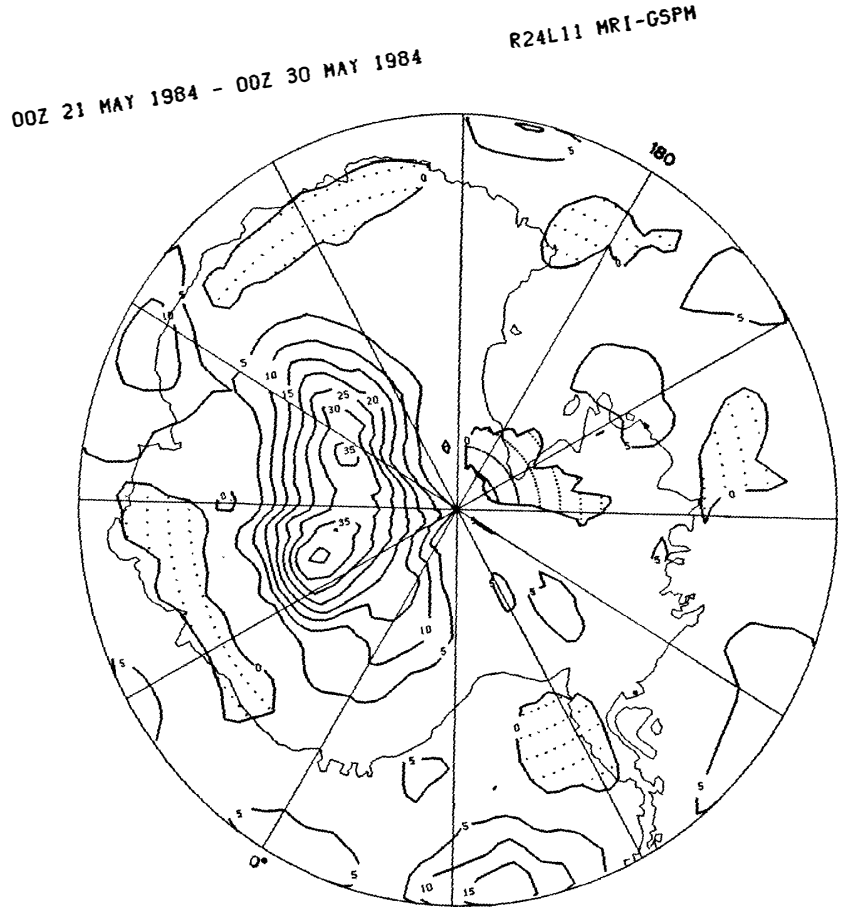

Fig. 8(a).

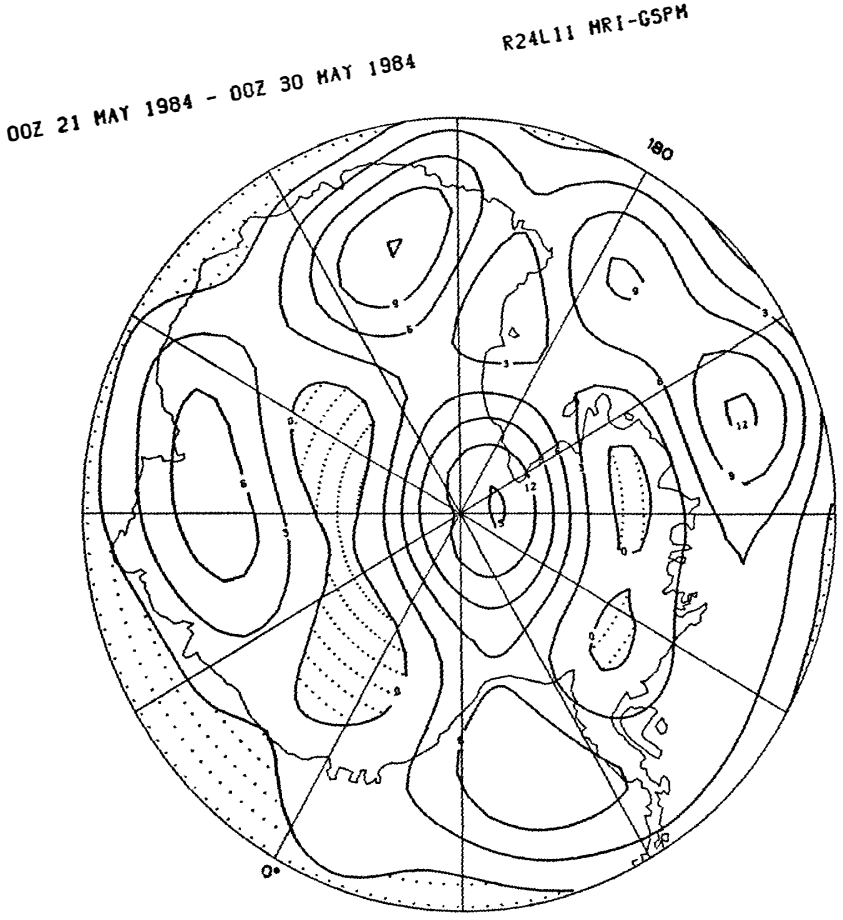

Fig. 8(b).

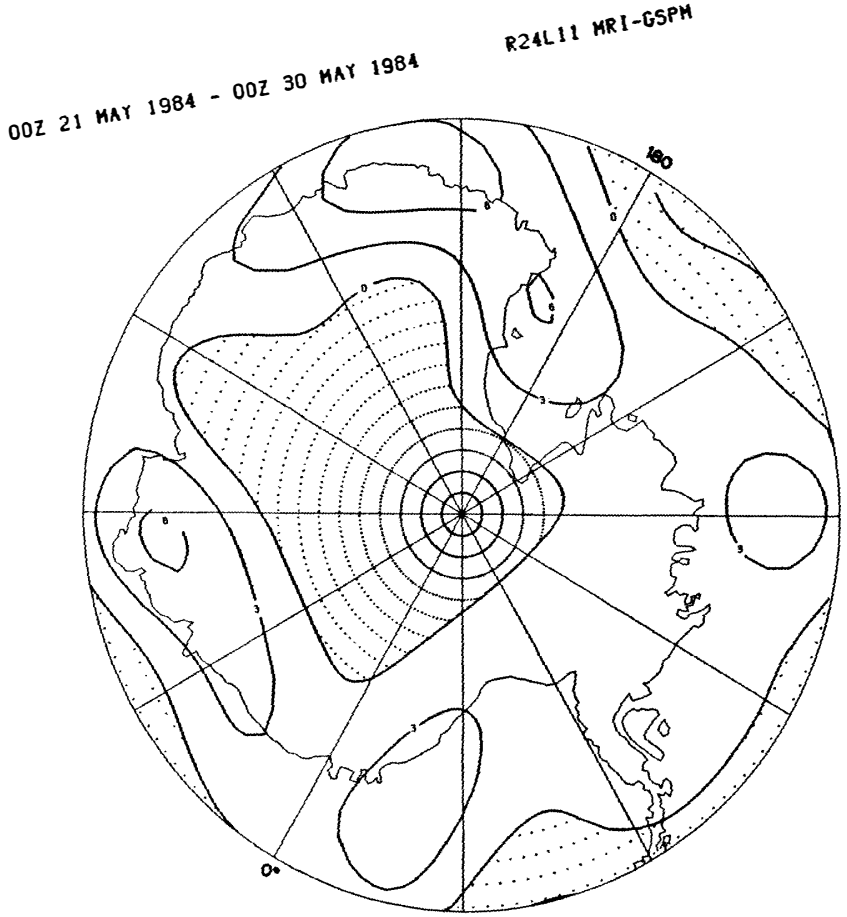

Fig. 8(c).

Fig. 8. (a) *Vertical temperature difference between the lowest level of* $\sigma=0.99$ *and the surface* ($\sigma=1.00$) *in the third 10-day period. Contour interval is 3 K, and negative difference areas are dotted.* (b) *As in* (a) *but for between the levels of* $\sigma=0.94$ *and 0.99.* (c) *As in* (a) *but for between the levels of* $\sigma=0.84$ *and 0.94.*

as shown in Fig. 1.

When surface air mass goes down the Antarctic continental slopes, divergence and convergence occur as shown in Fig. 6. Strong convergence takes place in topographic valley regions. There are strong convergence regions over the Filchner and Ross Ice Shelves, and a weak convergence region is on the Amery Ice Shelf. As to divergence, similar correspondences hold; strong divergence takes place along the four topographic ridges in the East Antarctic, and along the two topographic ridges in the West Antarctic. Figure 6 also implicitly shows that subsidence of upper warmer air associated with divergence occurs in most parts of the Antarctic.

4.3. Surface inversion

The surface temperature map depicted in Fig. 7 shows that the surface temperature on the "east plateau" is very low; the minimum temperature is less than 200 K. Figures 8(a), (b) and (c) show temperature differences between neighboring levels for the lowest four levels. The temperature difference between the lowest ($\sigma=0.99$) and the surface ($\sigma=1.00$), $T(0.99)-T_g$, is very large on the "east plateau", its maximum value being 40 K, while it is small in other regions as shown in Fig. 8(a). The temperature difference between the lowest layer and the next layer, $T(0.94)-T(0.99)$, is negative on the "east plateau", and takes maximum values around the "east plateau" (Fig. 8(b)). The next temperature difference, $T(0.84)-T(0.94)$, shows negative values in a wider region, and maximum values in the regions nearer the coast (Fig. 8(c)), compared with the temperature difference in the lower levels, $T(0.94)-T(0.99)$. Consequently, the surface inversion is strong yet low on the "east plateau", while it is weak yet high in other regions, its height increasing with distance from the "east plateau". The maximum strength of the inversion on the "east plateau", 40 K, corresponds to longwave radiative equilibrium, *i.e.*, net longwave radiation flux=0 (YAMANOUCHI and KAWAGUCHI, 1984), and also agrees with the maximum inversion found from measurements (SCHWERDTFEGER, 1970). Hence, the "east plateau" is close to being in the longwave radiative equilibrium.

4.4. Diabatic heating

The near-surface air over the Antarctic continent is cooled by both radiation and sensible heat exchange with the cold surface and warmed by both adiabatic compression through down draft and entrainment of the upper warmer air. In other words, the diabatic cooling owing to radiation and diffusion including the entrainment is reduced by the adiabatic heating Figure 9 shows the zonal mean diabatic cooling in the third 10-day period. Note that because of the zonal averaging, the topography in the Antarctic is distorted in Fig. 9; the "east plateau", included in the region from 80° to 85°S, becomes lower than the region from 85° to 90°S. We can see in Fig. 9 that very strong diabatic cooling (about 8 K/day) occurs in the midst of the Antarctic continental slope (around 76° and 88°S). In the coastal area the diabatic cooling changes its sign, namely, the near-surface air is warmed by diabatic heating. A maximum diabatic heating (about 10 K/day) occurs just inside of the sea ice margin.

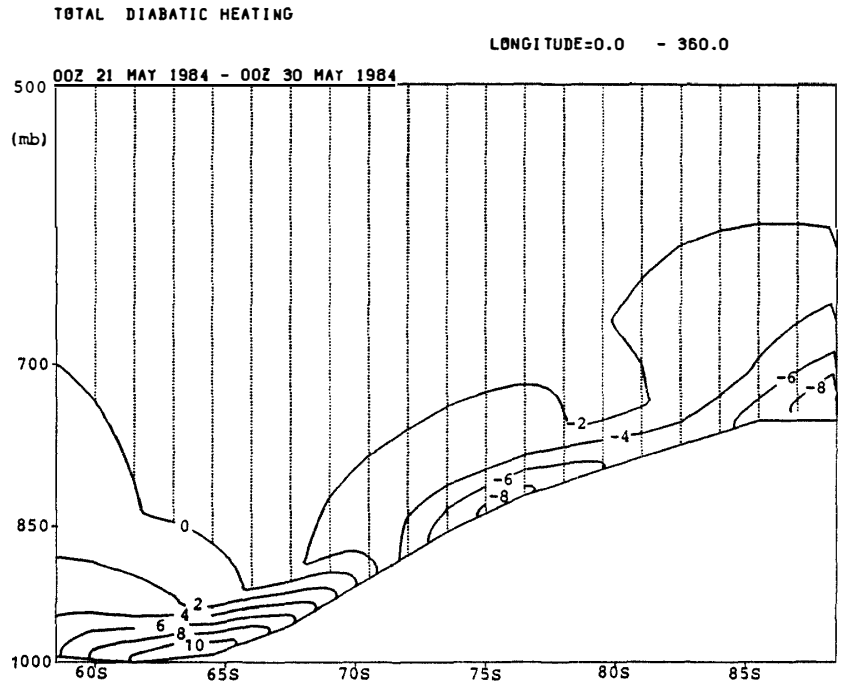

Fig. 9. Latitude-height section of the zonal mean diabatic heating in the third 10-day period. Contour interval is 2 K/day, and negative diabatic heating area is dotted.

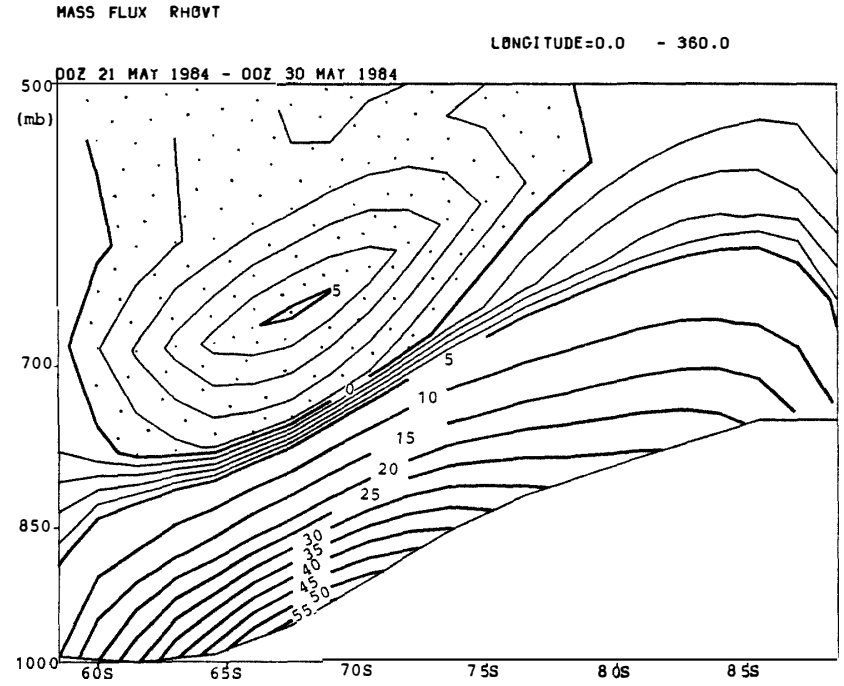

Fig. 10. Latitude-height section of the zonal mean mass flux in the third 10-day period. Contour interval is 0.1 kg/m²s in the region where absolute mass flux is less than 0.5kg/m²s, and it is 0.5 kg/m²s in the region where absolute mass flux exceeds 0.5 kg/m²s. Dotted area represents southward mass flux.

4.5. Meridional mass flux

Figure 10 shows the zonal mean mass flux, $[\bar{\rho}\cdot\bar{v}]$, where $\bar{\rho}$ and $\bar{v}$ are the 10-day means of air density and meridional velocity, respectively. We obtained a similar result even when we used daily data. The surface inversion layer of about 150 mb thickness exhibits intense mass flux out of the Antarctic. Above that layer there is weak poleward mass flux, in which relatively intense flux of about 100 mb thickness occurs just above the surface inversion layer. Since divergence dominates in the surface inversion layer (as shown in Fig. 6 for the lowest layer), warm air entrains from the layer of poleward flow to the surface inversion layer. This poleward flow is thought to correspond to the intense poleward vapor flow around 850 mb (BROMWICH, 1979), while there is no corresponding flow in the analysis of WHITE and BRYSON (1967).

5. Comparison of Runs A, B and C

5.1. Surface temperature

As expected from the difference in longwave downward fluxes (see Table 1), the surface temperature of run A is higher almost everywhere than that of run B, although it is not higher on the "east plateau". Figure 11 shows the zonal mean temperatures of the surface and the lowest layer ($\sigma=0.99$). The surface temperature of run C shows the lowest value. This is because the longwave downward flux is reduced through the effect of clouds. The cloud emissivity becomes 0.5 in the lower temperature range, $T<-60°C$, so that the cloud amount in run C is substantially half, or much less, of those in runs A and B over the Antarctic.

According to DOLGANOV (1986) the total cloud amount in the Antarctic approximately decreases with height, and so does the low level cloud amount. In spite of agreement with observations being poor in detail, the total cloud amount in the model is also small in the higher topographic region. Hence, we can roughly estimate the impact of cloud amount from the model results. According to observations in the katabatic wind zone (YAMANOUCHI and KAWAGUCHI, 1984) the change in longwave downward flux at the surface owing to overcast clouds is as follows: Middle or low level clouds increase the downward flux by about 80 W/m^2, and high level clouds about 40 W/m^2; These values are almost constant throughout the year. Also in the inner region overcast clouds increase the downward flux by a similar order unless clouds are thick. Since on the "east plateau" longwave net flux balances with sensible heat flux in the polar night, with its magnitude being about 15 W/m^2, cloud amount is expected to have a large effect on the surface temperature. That is, if colud amount in the model is far from that of the observations, so is the surface temperature. Run C thus corresponds to the case of less cloud amount and lower surface temperature.

The surface air temperature exhibits, similarly to the surface temperature, the highest value in run A and the lowest value in run C as shown in Fig. 11. The relatively high temperatures about 80°S in Fig. 11, which correspond to the temperature on the "east plateau", indirectly show the subsidence of upper warm air.

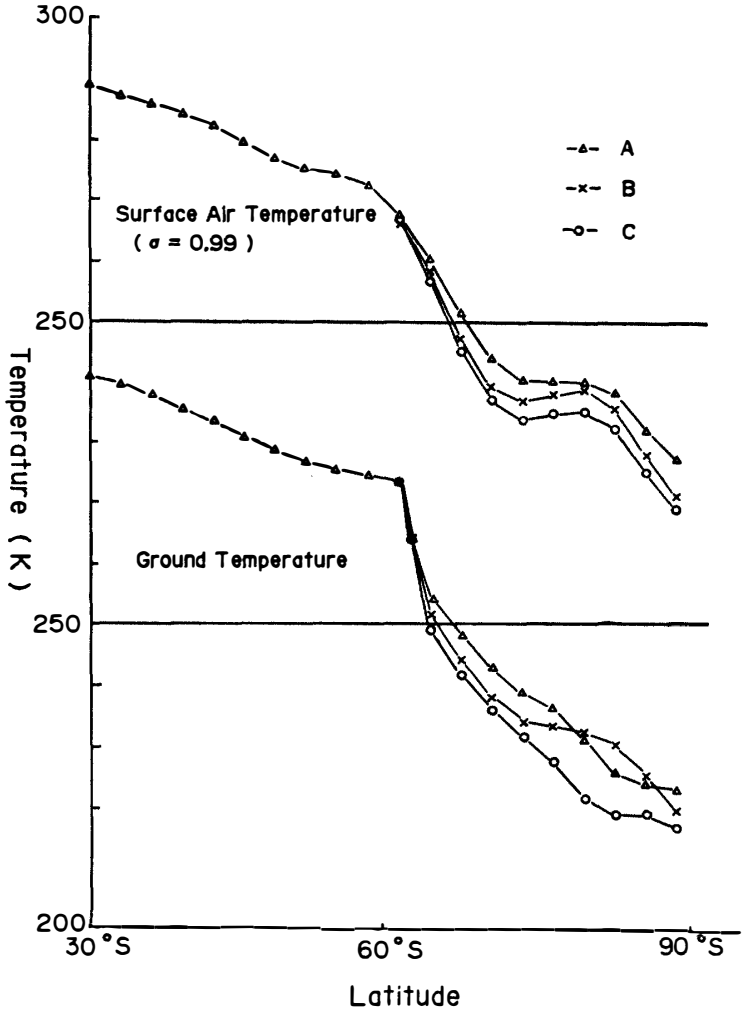

Fig. 11. Latitudinal distribution of the zonal mean temperatures of surface air and ground surface in the third 10-day period. The symbols, —△—, —×— and —○— represent runs A, B and C, respectively.

5.2. Surface wind

The surface winds show nearly similar directions in the three runs A, B and C, although there are some differences among them in the coastal area according to the positions and intensities of the circumpolar lows. The surface wind speeds of run B are comparable to those of run A, while those of run C are much larger than those of run A. The surface divergence and vorticity in run B are slightly larger than those in run A, and those in run C are the largest. In all the three runs the patterns of surface divergence and vorticity conform to the topography. Considering the similarity of surface wind directions and the difference of surface wind speeds in the three runs, we can say that the surface wind streamline is mainly determined by the direction of the pressure gradient along the surface. This is the reason why simple inversion models can approximately simulate the surface winds (MANNOUJI, 1984; EGGER, 1985; PARISH and BROMWICH, 1986, 1987).

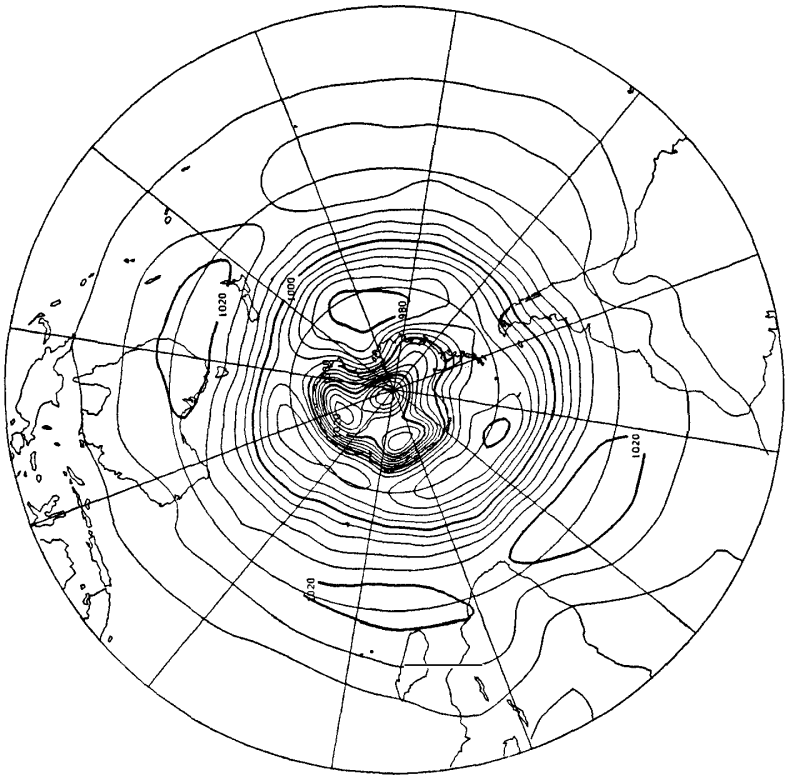

Fig. 12(b).

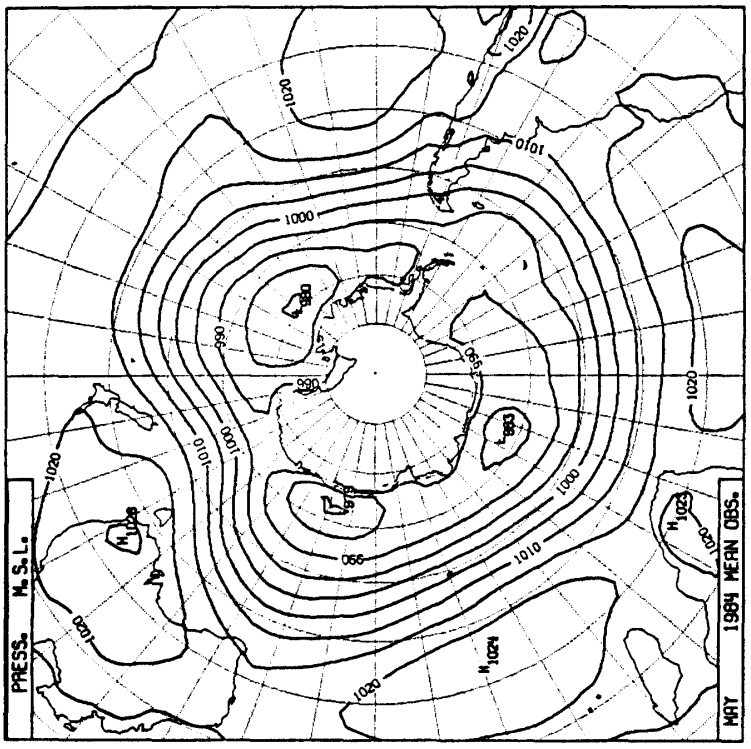

Fig. 12(a).

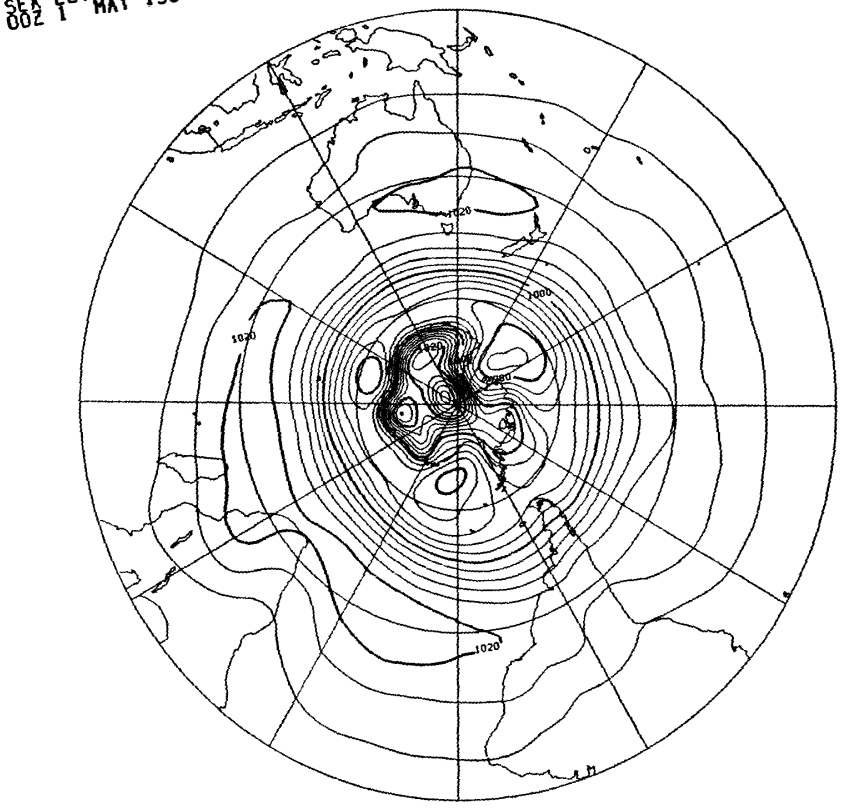

Fig. 12(c).

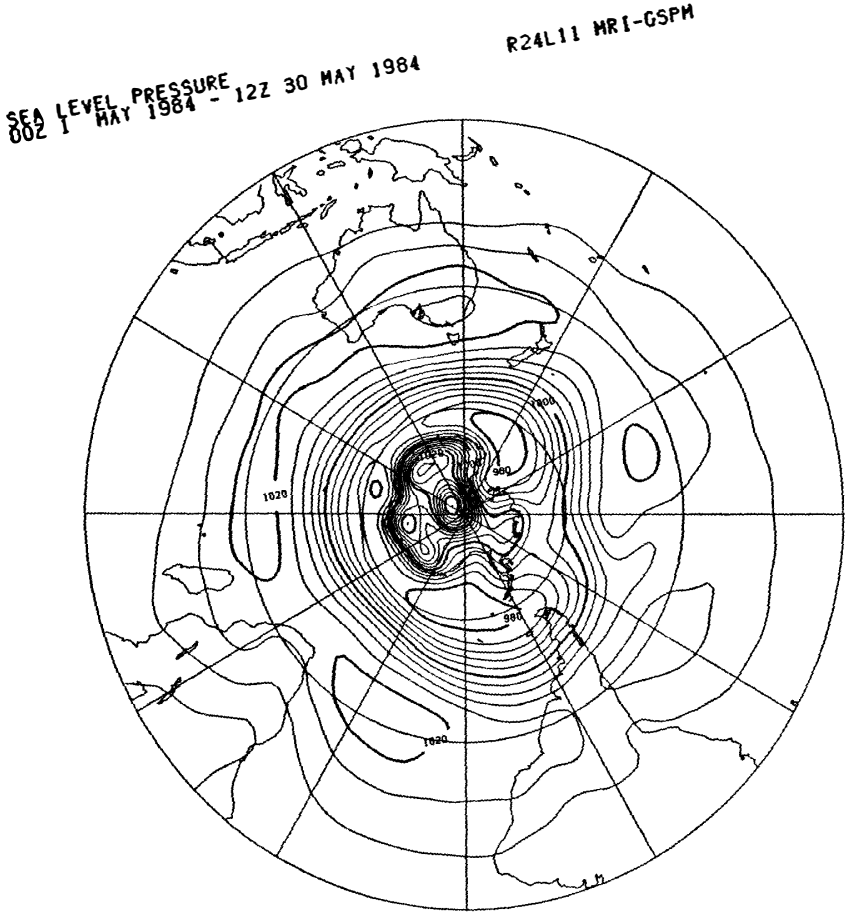

Fig. 12(d).

Fig. 12. (a) ECMWF analysis of monthly mean surface pressure. Contour interval is 5 mb. (b) Monthly mean surface pressure of run A. Contour interval is 4 mb. (c) As in (b) but for run B. (d) As in (b) but for run C.

5.3. Surface pressure

Figure 12(a) shows the surface pressure analysis of the European Centre for Medium Range Weather Forecasts (ECMWF, 1985) and Figs. 12(b), (c) and (d) show the simulated surface pressures of the three runs. The three cells of the circumpolar lows are reproduced in all runs, but there are some systematic differences; in run C the circumpolar lows are nearest the Antarctic Continent with the lowest pressures, while in run A they are farthest from the Antarctic Continent with the highest pressures. Compared with the analysis of ECMWF, runs B and C have relatively large errors that the sea level pressure is too low in the Weddell Sea and the Ross Sea. On the other hand, the surface pressure over the Antarctic Continent is lowest in run C and highest in run A. In particular, the difference between run A and run B or C is

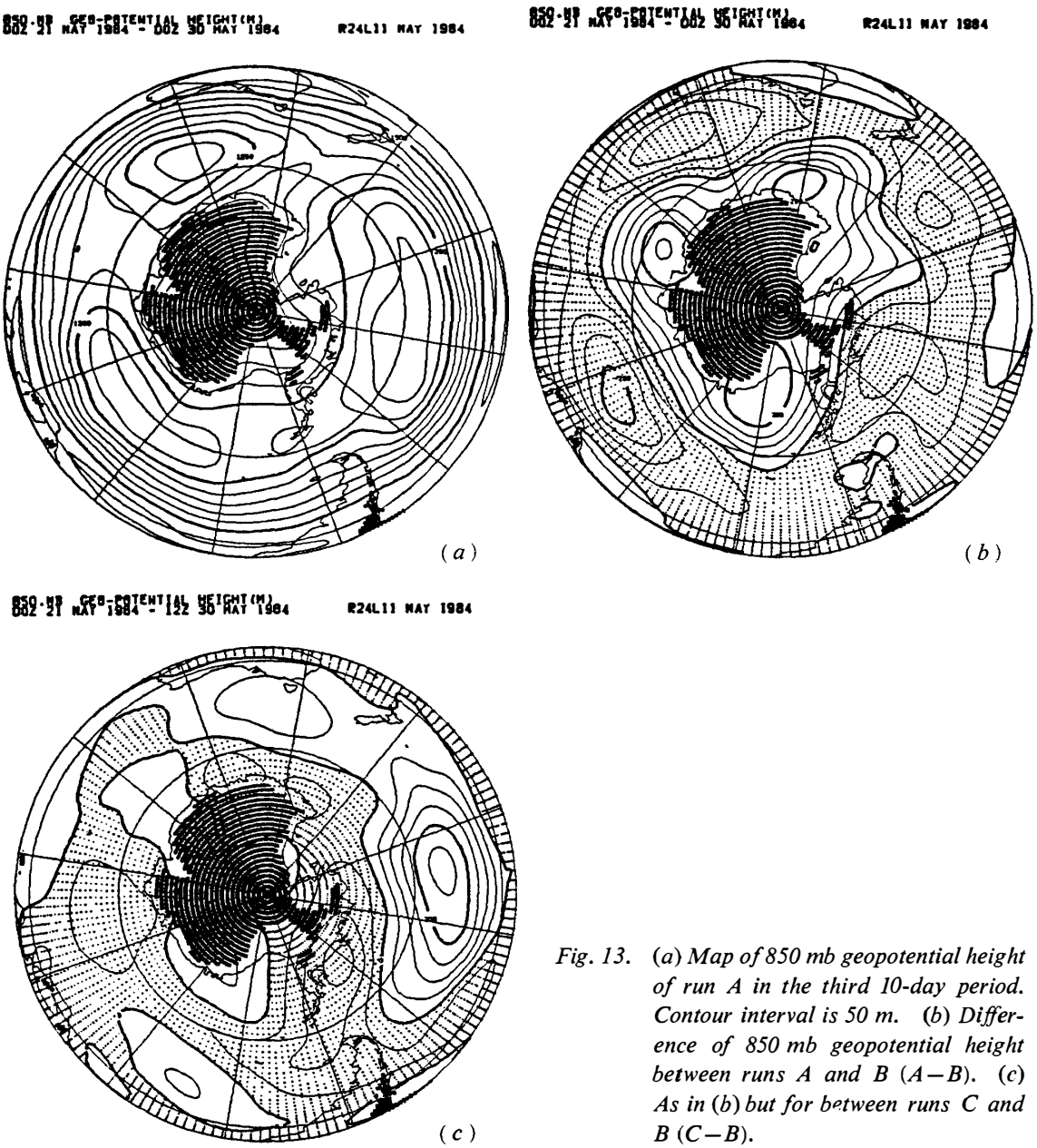

Fig. 13. (a) Map of 850 mb geopotential height of run A in the third 10-day period. Contour interval is 50 m. (b) Difference of 850 mb geopotential height between runs A and B (A−B). (c) As in (b) but for between runs C and B (C−B).

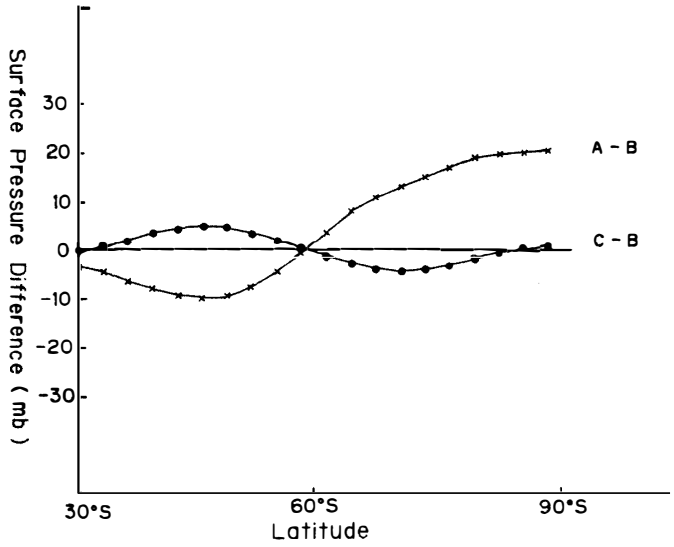

Fig. 14. Latitudinal distribution of the difference in the zonal mean surface pressures in the third 10-day period. The symbols —×— and —●— represent differences between runs A and B, and runs C and B, respectively.

very large over the Antarctic Continent and its zonal mean value amounts to about 20 mb as will be shown later. A similar large difference can be seen in geopotential heights of the lower troposphere as shown in the 850 mb geopotential height maps (Figs. 13(a), (b) and (c)). In accordance with these changes the baroclinic zone moves south- or northward; in run A it is located at the northernmost latitude, while in run C at the southernmost latitude.

These changes in surface pressures can be seen more clearly in the zonal mean fields (Fig. 14). The pressure differences in the Antarctic (higher latitudes than 60°S) show opposite sense to those in the sea around it (lower latitudes than 60°S). We can see from the differences in the surface temperatures (Fig. 11) and those in the surface pressures (Fig. 14) that the surface pressure over the Antarctic is closely correlated to the surface temperature; When the surface temperature over the Antarctic rises, the surface pressure also rises, and the circumpolar lows move northward while weakening.

6. Summary and Concluding Remarks

We have run a global spectral model of the MRI for one month, May, and examined the effects of radiation schemes including cloud emissivity on the surface temperature and wind over the Antarctic and on the pressure fields in the polar region.

The longwave net radiation is nearly balanced with the sensible heat flux over the Antarctic Continent. The sensible heat flux takes minimum values on the two highlands in the East and West Antarctic, and maximum values in the midst of the continental slope around these two highlands.

The temperatures of surface air and surface are largely affected by cloud amount (emissivity). When cloud amount decreases, the surface temperature becomes very low and so does the surface air temperature.

The surface velocity potential and stream function are approximately of similar orders and conform to the topography, so that the divergent wind and rotational wind are also comparable to each other, and the surface air mass flows out while descending and rounding the Antarctic Continent.

Intense mass flux out of the Antarctic occurs in the surface inversion layer. Above the surface inversion layer there is weak mass flux into the Antarctic compensating for the surface mass flux. In addition, just above the surface inversion layer there is a thin (about 100 mb) layer, in which relatively large mass flows into the Antarctic, and the warm air from this layer is entrained into the lower inversion layer according to the surface divergence.

The three runs can yield similar surface wind patterns, which coincide in large scale with the climatological streamline field of MATHER and MILLER (1967). Hence, the surface wind direction hardly depends upon the surface temperature. On the other hand, the surface wind speed decreases as the surface air temperature rises and so do the surface divergence and vorticity.

The pressure field in the polar region is closely connected to the surface temperature over the Antarctic. When the surface air temperature lowers, the surface pressure over the Antarctic decreases, but the surface pressure over the sea around the Antarctic increases. In accordance with these changes the circumpolar lows move poleward and their intensities are enhanced.

Acknowledgments

The authors wish to express their thanks to S. CHUBACHI and M. SHIOBARA for invaluable comments. Calculations were performed with the HITAC S-810/10 and M-280D computers in the Meteorology Research Institute.

References

BALL, F. K. (1956): The theory of strong katabatic winds. Aust. J. Phys., **9**, 373–386.

BROMWICH, D. H. (1979): Precipitation and accumulation estimates for East Antarctica, derived from rawinsonde information. Research Report, Department of Meteorology, University of Wisconsin, 142 p.

CHIBA, M., KIDA, H., FUKUTANI, H., TANAKA, Y., KAWAHARA, M., YAMADA, S. and UENO, T. (1986): A simulation of seasonal change of the atmospheric general circulation with a low resolution spectral model. Part I; Calculated monthly mean fields. Meteorol. Geophys., **37**, 53–82.

CHOU, M. D. and PENG, L. (1983): A parameterization of the absorption in the 15 μm CO_2 spectral region with application to climate sensitivity studies. J. Atmos. Sci., **40**, 2183–2192.

DALRYMPLE, P. (1966): A physical climatology of the Antarctic Plateau. Studies in Antarctic Meteorology, ed. by M. J. RUBIN. Washington, D. C., Am. Geophys. Union, 195–231.

DOLGANOV, L.V. (1986): Atmosfernye usloviya yuzhnoy polyarnoy oblasti (Atmospheric Conditions of the Southern Polar Region), Leningrad, Gidrometeoizdat, 176 p.

ECMWF (1985): Daily Global Analyses April–June 1984. Reading, European Centre for Medium Range Weather Forecasts.

EGGER, J. (1985): Slope winds and the axisymmetric circulation over Antarctica. J. Atmos. Sci., **42**, 1859–1867.

GRIFFITH, K. T., COX, S. K. and KNOLLBERG, R. G. (1980): Infrared radiative properties of tropical

cirrus clouds inferred from aircraft measurements. J. Atmos. Sci., **37**, 1077–1087.

HARSHVARDHAN, DAVIES, R., RANDALL, D. A. and CORSETTI, T. G. (1987): A fast radiation parameterization for atmospheric circulation models. J. Geophys. Res., **92**, 1009–1016.

HERMAN, G. F. and JOHNSON, W. T. (1980): Arctic and Antarctic climatology of a GLAS general circulation model. Mon. Weather Rev., **108**, 1974–1991.

HOLLOWAY, J. L., Jr. and MANABE, S. (1971): Simulation of climate by a global general circulation model; I. Hydorological cycle and heat balance. Mon. Weather Rev., **99**, 335–370.

KATAYAMA, A. (1972): A simplified scheme for computing radiative transfer in the troposphere. Technical Report No. 6, Department of Meteorology, University of California, 77 p.

KIEHL, J. T. and RAMANATHAN, V. (1983): CO_2 radiative parameterization used in climate models; Comparison with narrow band models and with laboratory data. J. Geophys. Res., **88**, 5191–5202.

KUHN, M., KUNDLA, L. S. and STRESCHEIN, L. A. (1977): The radiation budget at Plateau Station, Antarctica, 1966–1967. Meteorological Studies at Plateau Station, Antarctica, ed. by J. A. BUSINGER. Washington, D.C., Am. Geophys. Union, 41–73.

LACIS, A. A. and HANSEN, J. E. (1974): A parameterization for the absorption of solar radiation in the earth's atmosphere. J. Atmos. Sci., **31**, 118–133.

LIOU, K. N. (1974): On the radiative properties of cirrus in the window region and their influence on remote sensing of the atmosphere. J. Atmos. Sci., **31**, 522–532.

MANABE, S. and HAHN, D. G. (1981): Simulation of atmospheric variability. Mon. Weather Rev., **109**, 2260–2286.

MANNOUJI, N. (1984): A numerical experiment on katabatic wind with a two-dimensional axial symmetric model. Mem. Natl Inst. Polar Res., Spec. Issue, **34**, 233.

MATHER, K. B. and MILLER, G. S. (1967): Note on topographic factors affecting the surface wind in Antarctica, with special reference to katabatic winds; And bibliography. Technical Report UAG-R-189, University of Alaska, 125 p.

MCCLATCHEY, R. A., FENN, R. W., SELBY, J. E. A., VOLZ, F. E. and GARING, J. S. (1972): Optical Properties of the Atmosphere, 3rd, ed., Rep. AFCRL-72-0497, Bedford, MA, Air Force Geophysics Laboratory, 108 p.

PARISH, T. and BROMWICH, D. (1986): The inversion wind pattern over West Antarctica. Mon. Weather Rev., **114**, 849–860.

PARISH, T. and BROMWICH, D. (1987): The surface windfield over the Antarctic ice sheets. Nature, **328**, 51–54.

PITCHER, E. J., MALONE, R. C., RAMANATHAN, V., BLACKMON, M. L., PURI, K. and BOURKE, W. (1983): January and July simulations with a spectral general circulation model. J. Atmos. Sci., **40**, 580–604.

RAMANATHAN, V., PITCHER, E. J., MALONE, R. C. and BLACKMON, M. L. (1983): The response of a spectral general circulation model to refinements in the radiative processes. J. Atmos. Sci., **40**, 605–630.

RUSIN, N. P. (1964): Meteorological and Radiational Regime of Antarctica. Jerusalem, Israel Program for Scientific Translations, 355 p.

SCHLESINGER, M. E. (1984): Atmospheric general circulation model smulations of the modern Antarctic climate. Environment of West Antarctica; Potential CO_2-Induced Changes. Washington, D.C., National Academy Press, 155–196.

SCHWERDTFEGER, W. (1970): The climate of the Antarctic. Climates of the Polar Regions, ed. by S. ORVIG. Amsterdam, Elsevier, 253–355.

SHIBATA, K. and AOKI, T. (1989): An infrared radiative scheme for the numerical models of weather and climate. J. Geophys. Res., **94**, 14923–14943.

SHIBATA, K., CHIBA, M. and AOKI, T. (1988): Chôha-hôsha no Katayama sukîmu no gosa ni tsuite (On the errors of the longwave radiative transfer scheme of Katayama). Zenkoku Chôki Yohô Kentôkai Shiryô (Technical Report on the Long Range Forecasts), Meteorological Research Institute, 31–37.

STEPHENS, G. L. (1978): Radiation profiles in extended water clouds. II; Parameterization schemes. J. Atmos. Sci., **35**, 2123–2132.

WELLER, G. (1969): A meridional surface wind speed profile in MacRoberson Land, Antarctica. Pure Appl. Geophys., **77**, 193–200.

WHITE, F. D., Jr. and BRYSON, R. A. (1967): The radiative factor in the mean meridional circulation of the Antarctic atmosphere during the polar night. WMO Technical Note, **87**. Geneva, World Meteorological Organization, 199–224.

YAMAMOTO, G. (1952): On a radiation chart. Sci. Rep. Ser. 5, Geophys., **4**, 9–23.

YAMAMOTO, G., TANAKA, M. and ASANO, S. (1970): Radiative transfer in water clouds in the infrared region. J. Atmos. Sci., **27**, 282–292.

YAMANOUCHI, T. and KAWAGUCHI, S. (1984): Longwave radiation balance under a strong surface inversion in the katabatic wind zone, Antarctica. J. Geophys. Res., **89**, 11771–11778.

(*Received November 14, 1988; Revised manuscript received May 19, 1989*)